Dynamics of Atmospheres and Oceans 63 (2013) 1–23

Contents lists available at SciVerse ScienceDirect

Dynamics of Atmospheres and Oceans

journal homepage: www.elsevier.com/locate/dynatmoce

A MITgcm/DART ensemble analysis and prediction system with application to the Gulf of Mexico

Ibrahim Hoteit[a,*], Tim Hoar[b], Ganesh Gopalakrishnan[c], Nancy Collins[b], Jeffrey Anderson[b], Bruce Cornuelle[c], Armin Köhl[d], Patrick Heimbach[e]

[a] *King Abdullah University of Science and Technology (KAUST), Thuwal, Saudi Arabia*
[b] *National Center of Atmospheric Research (NCAR), Boulder, CO, USA*
[c] *Scripps Institution of Oceanography, University of California, San Diego, USA*
[d] *Institute of Oceanography, University of Hamburg, Hamburg, Germany*
[e] *Massachusetts Institute of Technology (MIT), Boston, MA, USA*

ARTICLE INFO

Article history:
Received 29 November 2011
Received in revised form 23 March 2013
Accepted 26 March 2013
Available online xxx

Keywords:
Data assimilation
Ocean state estimation
Ensemble Kalman filter
Gulf of Mexico

ABSTRACT

This paper describes the development of an advanced ensemble Kalman filter (EnKF)-based ocean data assimilation system for prediction of the evolution of the loop current in the Gulf of Mexico (GoM). The system integrates the Data Assimilation Research Testbed (DART) assimilation package with the Massachusetts Institute of Technology ocean general circulation model (MITgcm). The MITgcm/DART system supports the assimilation of a wide range of ocean observations and uses an ensemble approach to solve the nonlinear assimilation problems. The GoM prediction system was implemented with an eddy-resolving 1/10th degree configuration of the MITgcm. Assimilation experiments were performed over a 6-month period between May and October during a strong loop current event in 1999. The model was sequentially constrained with weekly satellite sea surface temperature and altimetry data. Experiments results suggest that the ensemble-based assimilation system shows a high predictive skill in the GoM, with estimated ensemble spread mainly concentrated around the front of the loop current. Further analysis of the system

* Corresponding author. Tel.: +966 544700033.
E-mail address: ibrahim.hoteit@kaust.edu.sa (I. Hoteit).

0377-0265/$ – see front matter
http://dx.doi.org/10.1016/j.dynatmoce.2013.03.002

estimates demonstrates that the ensemble assimilation accurately reproduces the observed features without imposing any negative impact on the dynamical balance of the system. Results from sensitivity experiments with respect to the ensemble filter parameters are also presented and discussed.

1. Introduction

The Gulf of Mexico (GoM) is a semi-enclosed basin which connects to the Caribbean Sea to the south through a narrower and deeper (about 2000 m deep and 200 km wide at the surface) "V"-shaped Yucatan Channel (YC) between the Yucatan Peninsula (west) and Cuba (east), and to the Atlantic Ocean to the east through a relatively narrower and shallower (about 900 m deep and 100 km wide at the surface) Straits of Florida. The circulation in the GoM is dominated by the energetic Loop current (LC) which connects the Caribbean sea, GoM, and the Straits of Florida. The Caribbean current from the south flows northward through the YC into the GoM and takes a sharp 90° turn, looping eastward, resulting in the formation of the LC. The LC carries warm and saline waters into the GoM and continues to flow northward as the major component of the Gulf stream and the Florida current along the Straits. The LC is the major source of energy, variability, and momentum, driving most of the circulation within the GoM (Ohlmann et al., 2001). The LC dynamics are associated with the LC extension, retraction, and separation of large anti-cyclonic LC eddies (LCE), which shed into the GoM at irregular intervals with a shedding interval ranging between 3 and 11 months (Oey et al., 2005b; Leben, 2005). The LCE, with an eddy size of 200–400 km, and vertical extent of about 1000 m, propagates predominantly westward at a speed of 2–5 km day^{-1} with an *e*-folding eddy decay time-scale of approximately 1 year (e.g. Vukovich, 1995; Oey et al., 2005b). The mechanism responsible for the LCE shedding is often explained by the momentum imbalance paradox (Nof, 2005). A detailed review of LC dynamics and GoM circulation can be found in Oey et al. (2005b).

Oil exploration in the deep GoM is vulnerable to hazards due to strong currents at the fronts of the highly nonlinear warm-core eddies. The LC has complex variability and the occasional LCE detachment and reattachment make it very difficult to clearly define, identify, monitor, and forecast an eddy shedding event. The predictability of LCE shedding events in the GoM therefore poses a major challenge for the Oil and Gas industry. A three-dimensional ocean forecasting system for the GoM capable of an accurate 1–2 weeks LC forecast is highly desired by the Oil and Gas industry and would provide enough time for efficient planning of their operations. The development of such a system requires an ocean general circulation model (OGCM) capable of simulating the GoM circulation and an efficient assimilation scheme that, given enough observations, provides accurate initial conditions for forecasting (Ghil and Malanotte-Rizzoli, 1991; Wunsch, 1996; Bennett, 2002). By combining these two sources of information, one can obtain the most complete description of the changing ocean, which would not have been possible to obtain from either the model or the data alone (Stammer and Chassignet, 2000).

The theoretical framework of ocean data assimilation is now well established and two separate directions are usually followed; one being a variational approach, and the other being a Bayesian estimation approach. Under some assumptions (mainly Gaussianity and linearity), both approaches could be simplified to very similar algorithms. Variational methods seek the model trajectory which best fits available data by minimizing the discrepancy between the model simulation and observations while adjusting a well-chosen set of uncertain model parameters (Le Dimet and Talagrand, 1986). Bayesian methods (e.g. nudging, optimal interpolation (OI), and Kalman filter) usually proceed by incrementally correcting a model prediction every time new observations are available, based on prior information about uncertainties in the model and data. In the ensemble Kalman filters (EnKFs) Monte Carlo techniques are used to integrate the uncertainties with the full nonlinear model before applying the Kalman correction (Tippett et al., 2003).

Early data assimilation studies in the GoM mainly used the Princeton Ocean Model (POM) with different assimilation schemes and a variety of data sets. For instance, a simple nudging was used by Kantha et al. (2005) to assimilate sea surface height (SSH) and sea surface temperature (SST) data. Near-surface model corrections were projected into sub-surface density using surface/sub-surface correlations (Oey et al., 2005a). A similar system was used by Fan et al. (2004) to assimilate drifter tracks along with SST/SSH data. A combination of nudging and an OI scheme was used by Lin et al. (2007). Application of ensemble methods to forecast LCE in the GoM was implemented by Yin and Oey (2007), where SST/SSH data were first assimilated using a 3DVAR technique to compute an initial analysis, and a bred-ensemble forecast was then used to generate an initial analysis ensemble for forecasting. More recently, GoM assimilation studies investigated the Hybrid Coordinate Ocean Model (HYCOM). Chassignet et al. (2007), Srinivasan et al. (2001) implemented OI-based schemes to assimilate a variety of data into HYCOM. A series of Ensemble OI-based studies were reported by Counillon and Bertino (2009a,b) assimilating mapped satellite sea level anomaly data. 4DVAR-based assimilation systems were also recently implemented in the GoM. For instance, the cyclic representer algorithm for the variational method was used by Ngodock et al. (2007) with a 1.5 layer reduced gravity ocean model. Powell et al. (2008) implemented the ROMS-4DVAR assimilation system constraining the model with SSH/SST and in situ current data. A reduced-order variational approach has been also tested by Yu et al. (2009) using the Navy Coastal ocean Model (NCOM).

All the described GoM assimilation systems are either OI- or variational-based systems that are generally based on time-invariant background error covariance. In a recent study similar in objective to Hoteit et al. (2002) and Counillon et al. (2009) investigated the EnKF in the GoM with a limited ensemble to assess the benefit of adding a static covariance to the EnKF flow-dependent covariance following a hybrid EnKF/OI approach. The GoM assimilation system we present in this work is the first comprehensive implementation/evaluation of an ensemble-based Kalman filter in a realistic setup assimilating along-track satellite data.

We first describe the development of a state-of-the-art ensemble-based nonlinear ocean data assimilation system capable of assimilating most types of ocean observations in Section 2. The system is composed of the Data Assimilation Research Testbed (DART) assimilation package, a software facility employing different (stochastic and deterministic) EnKFs, and the Massachusetts Institute of Technology ocean general circulation model (MITgcm). Details of implementation of the MITgcm/DART assimilation system in the GoM and a complete evaluation of its performances are then presented in Section 3. Assimilation experiments are performed over a 6-month period during a strong loop current event in 1999. A 1/10th degree configuration of the MITgcm was sequentially constrained with weekly satellite sea surface temperature and altimetry data. We discuss the overall performance of the MITgcm/DART system and assess its forecasting skills in the GoM. We present and analyze results from sensitivity experiments with respect to different assimilation parameters and setups such as the ensemble size, localization scale, and assimilated data. We also study the impact of the sequential EnKF correction steps on the dynamical balance of the GoM estimates. This is important to ensure that the linear Kalman correction of the EAKF does not distort the dynamical balance of the ocean estimates. A summary and a general discussion conclude the paper in Section 4.

2. The MITgcm/DART ocean assimilation system

The MITgcm and its adjoint incorporates the Estimation of the Circulation and the Climate of the Ocean (ECCO) state estimation infrastructure (Heimbach et al., 2002). The primary goal of the ECCO consortium is to provide the best possible dynamically consistent analysis of the large scale ocean circulation, which can serve as a basis for studies of elements important to climate (e.g. heat fluxes and variability). The primary purpose of integrating DART and the MITgcm is to develop accurate forecasting capabilities for the energetic mesoscale eddy fields, encompassing the establishment of global and real-time ocean forecasting systems with EnKF-based data assimilation techniques that can be efficiently executed on massively parallel computers.

2.1. MITgcm

The MITgcm is designed to study both large-scale/global and small-scale/regional ocean processes. The model integrates the Reynolds-averaged (or Navier–Stokes) equations on a sphere under the Boussinesq approximation (Marshall et al., 1997). It can be run in a non-hydrostatic mode. The equations are written in z-coordinates and discretized using finite difference approximations on a staggered "Arakawa C-grid". The model is endowed with state-of-the-art physical parameterization schemes for subgrid-scale horizontal and vertical mixing of momentum and tracer properties, and an atmospheric boundary layer scheme over the open ocean. The horizontal subgrid-scale mixing is parameterized with a constant eddy viscosity or nonlinear Smagorinsky viscosities. Diffusive and viscous operators are of second and fourth order. The K-Profile Parameterization (KPP) scheme of Large et al. (1994) is used for near-surface vertical diffusion and non-local transport coefficients. A variety of tracer advection schemes spanning from second to fourth order schemes are available. The model includes linear and polynomial equation of state formulas (McDougall et al., 2003). The model code and documentation are available on the MITgcm webpage http://mitgcm.org/.

2.2. DART

DART is a portable software facility employing different (stochastic and deterministic) EnKFs (Anderson et al., 2009). It has been developed at the National Center of Atmospheric Research (NCAR) and is now used for different operational weather forecasting problems (Zubrow et al., 2008; Aksoy et al., 2009; Dowell and Wicker, 2009, to cite but a few). An EnKF data assimilation system (also called a "filter") combines prior estimates of the observations derived from an ensemble of short-term model forecasts, the observation, and the observation error covariance to compute increments that are used to adjust the model forecasts. The filter exploits the sample covariance of the ensemble to determine how observations affect the model state.

DART is designed so that incorporating new models and new observation types requires minimal coding of a limited set of interface routines, and does not require modification of the existing model code. Forward operators for new observation types usually require a small set of interface routines and can be created nearly independently of the forecast model. DART includes a variety of algorithms for computing the updated ensemble, and a number of advanced inflation/localization methods essential for high quality performance of an ensemble data assimilation system (Anderson et al., 2009). Whereas localization tries to eliminate the spurious impact of observations from sampling error caused by small ensembles, inflation ensures the variance of the ensemble is consistent with the estimates derived from comparison of the forecasts with new data. Applications of DART also include parameter estimation, sensitivity analysis, observing system design, and smoothing.

DART includes a parallel version of the sequential ensemble filter using the message passing interface (MPI) programming model. The scaling characteristics of the algorithm are designed to be independent of the model and observations being assimilated (Anderson and Collins, 2007). For sufficiently large models, the algorithm scales to an arbitrary number of processors. The distributed code includes many models with various levels of complexity, various sets of observations, and skeleton code to guide users in adding their own models or new observation types. The reader is referred to the DART webpage http://www.image.ucar.edu/DAReS/DART for further information.

2.3. Implementation of DART with the MITgcm

Implementing DART with the MITgcm requires the design of a set of interface routines that exchange information between the MITgcm and DART – both of which run as separate executables (Fig. 1). The system starts from an initial ensemble of states that capture the uncertainty of the initial state estimate. The MITgcm state variables are the three-dimensional temperature, salinity, and horizontal velocities, as well as the two-dimensional sea surface height. Given the observations and an ensemble of initial states, "filter" assimilates the observations, updates the states, and determines how far to advance the MITgcm to accommodate the next set of observations. The MITgcm is then used as the forecast model to advance each ensemble member (either in turn or all-at-once) to the time of the

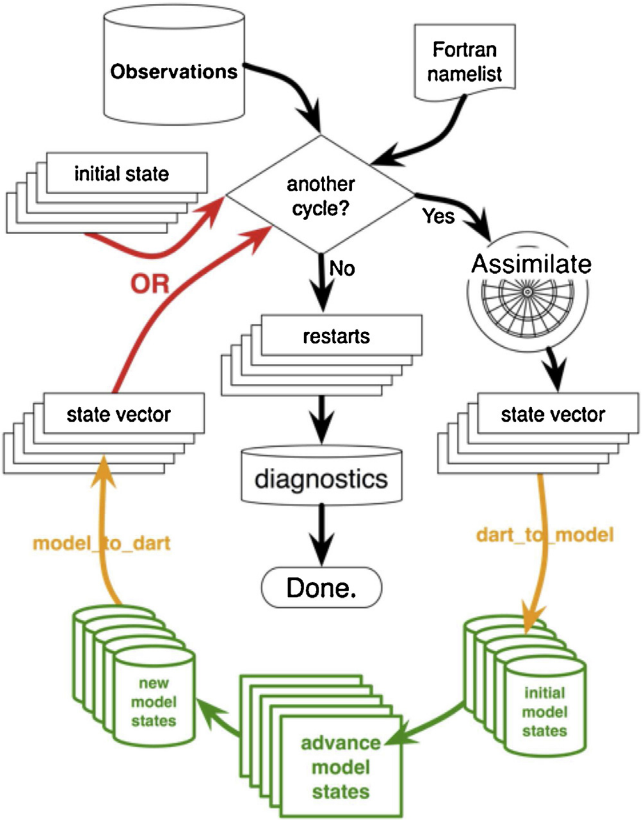

Fig. 1. A schematic description of the MITgcm/DART assimilation system. Starting at the top: observations, an ensemble of initial states, and control information are used to produce an collection of states that are consistent with the observations. The states are written to disk, as is the information needed to control the execution of the MITgcm. The states are converted to the form required by the MITgcm and advanced to the required time and written to disk. Those states are converted to a form required by DART and the process repeats. When there are no more observations or the control information is met, a set of restart files and a set of diagnostic files are written. The two interface routines "dart_to_model" and "model_to_dart" allow the use of the MITgcm code without modification.

next available observations. This forecast-update cycle continues as long as there are observations to assimilate or the namelist control is met. When that happens, a set of restart files (suitable to continue an experiment with more observations) and diagnostic files are written.

The MITgcm/DART assimilation system is now enabled for multivariate assimilation of most ocean data sets. This includes satellite surface temperature and altimetry data, in-situ temperature, salinity and velocity data, including high-frequency radar surface current measurements.

3. Application of the DART/MITgcm assimilation system in the Gulf of Mexico

3.1. MITgcm configuration in the Gulf of Mexico

The MITgcm was implemented in the GoM basin between 8.5° N and 31° N, and 262° E and 287.5° E on a $1/10^{\circ} \times 1/10^{\circ}$ grid with 40 vertical layers. The vertical resolution is spaced from 5 m at the surface to 300 m at depth, with spacing gradually increasing below to a maximum depth of 6000. The bathymetry is extracted from the 2-min gridded global topography ETOPO-2. The minimum water depth is set at 5 m. In this configuration, the model operates in a hydrostatic mode with an implicit free surface. No-slip conditions are imposed at the lateral boundaries while bottom friction is quadratic with a drag coefficient equal to 0.002. The subgrid-scale physics is approximated by a tracer second order diffusive operator in the vertical parameterized by the KPP model in the surface mixed layer. Background values of vertical diffusivity and viscosity are $1 \times 10^{-6}\,m^2/s$ and $1 \times 10^{-4}\,m^2/s$, respectively. In the horizontal, diffusive and viscous operators are of second and fourth order, respectively, with coefficients $1 \times 10^2\,m^2/s$ and $1 \times 10^{10}\,m^4/s$. No other parameterization of eddy mixing was used.

The GoM MITgcm is forced with daily means of the atmospheric state from the National Centers for Environmental Prediction (NCEP)/National Center for Atmospheric Research (NCAR) re-analysis project (Kalnay et al., 1996). This includes air temperature, specific humidity, wind speed, precipitation, and short and long wave radiative fluxes. Monthly climatological river run-off fluxes (freshwater) interpolated from a global $1^\circ \times 1^\circ$ field are also prescribed. Surface salinity is relaxed toward the monthly climatology (Levitus and Boyer, 1994) with a 30-day time-scale.

Eastern and northern open boundaries (OB) are set at 30.85° N and 287.55° E. In the MITgcm, temperature, salinity and the horizontal velocity components need to be specified along the OB. These were extracted from the 50-year ECCO 1°, known as GECCO, global state analysis as estimated by Köhl and Stammer (2008) using a global MITgcm and its adjoint and assimilating most of the available large-scale ocean data sets. The monthly means GECCO state estimates were spatially interpolated to the GoM model grid. The interpolated GECCO fields are prescribed at the grid points just outside the open boundary and the GoM model solution is relaxed to these values within a buffer zone of 1° over time scales varying linearly from 1 day at the boundary to 5 days at the edge of the zone. After interpolation, the GECCO normal velocity fields across the OB have been further adjusted to exactly balance the net volume flux into the GoM domain. More precisely, the transport bias between the interpolated GECCO (onto model grid) and the original GECCO, normalized by the total area of the vertical slice at the open boundary, was added to the interpolated GECCO, so that the net volume flux into the domain is zero.

The model was integrated over a 50-year period from 1952 to 2001 starting from the GECCO ocean global state estimate in January 1952. Comparison of model SSH mean and standard deviation from this model free-run with the estimated global mean dynamic topography by Rio and Hernandez (2004) and the SSH standard deviation from AVISO anomalies (Archiving Validation and Interpretation of Satellite Oceanographic Data, downloadable from the AVISO webpage at http://www.aviso.oceanobs.com/) is shown in Fig. 2. Same comparison for model SST mean and standard deviation with those from satellite TMI observations (TRMM – Tropical Rainfall Measuring Mission satellite – Microwave Imager downloadable from http://www.remss.com/tmi/tmi_description.html) is shown in Fig. 3. Note that for comparison with Rio and Hernandez (2004) mean SSH, the first 2 years of the model run were considered as a spin-up period, so the model SSH fields were averaged between 1954 and 2001. The comparison with AVISO anomalies and TMI is conducted over the period of data availability, i.e. between October 1992 and December 2001 for SSH, and January 1998 and December 2001 for SST. Overall, the model SSH mean is about right – showing similar patterns to that estimated by Rio and Hernandez (2004). The model SSH variability is weaker than what is observed by AVISO. The model captures most of the large SSH signal in the eastern GoM, particularly over the LC region. However, a slow than observed decay of the modeled LC eddies as they propagate westward likely causes a stronger SSH signature in the central GoM with an extended westward tail. The mean and variability of the model SST are also in quite good agreement with the TMI data. The model is generally warmer in the GoM, but the strong variability of the SST along the northern continental US coast is accurately depicted by the model. Further analysis of the fifty-year model simulations showed a realistic LC system and eddy shedding with a quasi-periodicity of 6–9 months. The model also represented the detachment and reattachment of the eddy with the LC system, and this phenomenon was observed at a period of about 3 months. These results are in rough agreement with earlier published results on the LC system and its developments (Oey et al., 2005b). The outcome of this free model run without assimilation suggests that the model is capable of simulating the variability of the GoM circulation and is therefore appropriate to be used for assimilation.

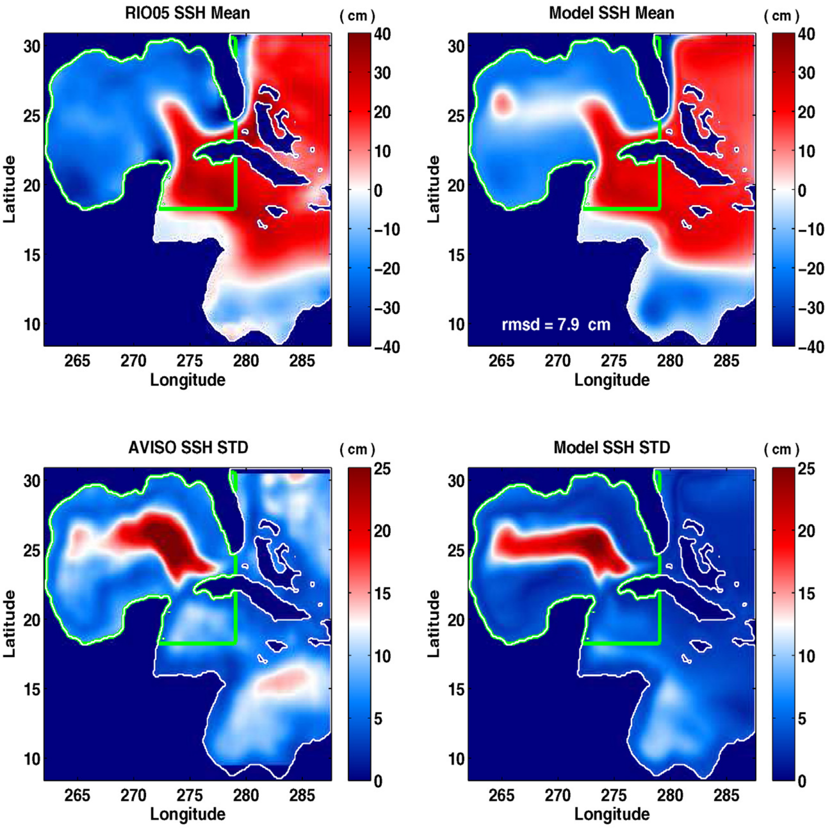

Fig. 2. SSH mean and standard deviation as simulated by the MITgcm free run between 1952 and 2001 compared to the SSH mean of Rio and Hernandez (2004) and SSH standard deviation of AVISO (units are cm). Green line marks the GoM domain. The horizontal RMS difference between the SSH mean fields is provided in the low left corner of the upper right panel. (For interpretation of the references to color in this figure legend, the reader is referred to the web version of the article.)

3.2. DART configuration for the Gulf of Mexico

Running DART with the MITgcm requires choosing the ensemble assimilation algorithm, the ensemble size, the localization length scale, and the inflation factor – as well as providing the initial ensemble.

Several variants of ensemble Kalman filters (EnKFs) have been introduced for data assimilation. These techniques are becoming increasingly popular because they are computationally tractable, allow nonlinear behavior in the forward model, have a flow-dependent prior covariance, and are readily expandable into an ensemble prediction system. EnKFs are commonly divided into stochastic and deterministic algorithms depending on whether the observations are perturbed, or not, before assimilation with noise sampled from the observational error statistics (Tippett et al., 2003). Perturbing the observations introduces noise to the system and could degrade the EnKF performance (Nerger et al., 2005; Hoteit et al., 2012). We use a deterministic EnKF, the ensemble adjustment Kalman filter (EAKF) initially described in Eqs. (14)–(16) of Anderson (2001).

The Data Assimilation Research Testbed (DART; Anderson et al., 2009) implementation of the EAKF is used here and makes a number of modifications to the algorithm for computational efficiency on scalable computing. The most important difference from the original EAKF algorithm is that observations are assimilated serially using the algorithm described in Anderson (2003). An observation, y, is assimilated by first computing its expected value $y_{p,n}$ by sampling each ensemble member using the

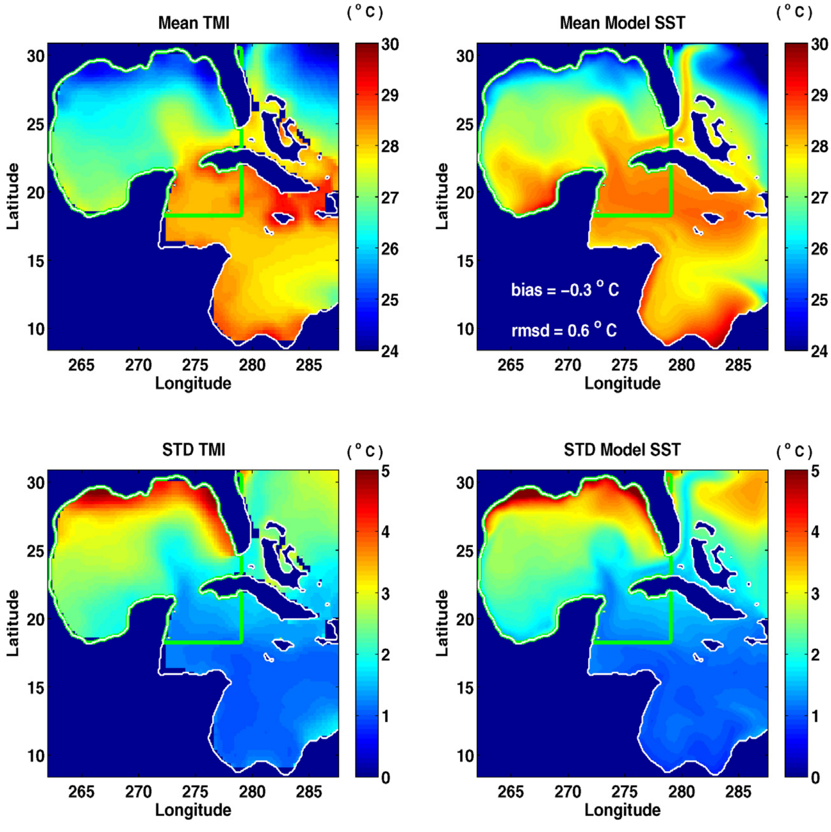

Fig. 3. SST mean and standard deviation as simulated by the MITgcm free run between 1952 and 2001 compared to the TMI SST mean and standard deviation (units are cm). Green line marks the GoM domain. The horizontal RMS difference between the SST mean fields and the associated horizontally averaged time-mean bias are provided in the low left corner of the upper right panel. (For interpretation of the references to color in this figure legend, the reader is referred to the web version of the article.)

observational operator relating the model state to the available observations. Here, $n = 1, \ldots, N$ and N is the ensemble size. If the sample mean and variance of this prior ensemble are $\bar{y}_p$ and σ_p^2, and the observed value and observational error variance are y^o and σ_o^2, the KF gives an updated variance

$$\sigma_u^2 = [(\sigma_p^2)^{-1} + (\sigma_o^2)^{-1}]^{-1} \tag{1}$$

and mean

$$\bar{y}_u = \sigma_u^2 \left(\frac{\bar{y}_p}{\sigma_p^2} + \frac{y^o}{\sigma_p^2} \right). \tag{2}$$

The updated ensemble estimate for y

$$\bar{y}_{u,n} = \left(\frac{\sigma_u^2}{\sigma_p} \right) (y_{p,n} - \bar{y}_p) + \bar{y}_u, \quad n = 1, \ldots, N, \tag{3}$$

is constructed by shifting the mean and linearly transforming the members to make the sample variance exactly σ_u^2 and the sample mean exactly $\bar{y}_u$.

Observation space increments resulting from assimilating the observation are defined as $\Delta y_n = y_{u,n} - y_{p,n}$. The ensembles of each of the models M state variables are then updated using the prior joint ensemble sample statistics so that

$$\Delta x_{m,n} = \left(\frac{\sigma_{xm,y}}{\sigma_p^2}\right)\Delta y_n \quad m = 1, \ldots, M, \quad n = 1, \ldots, N, \tag{4}$$

where $\sigma_{xm,y}$ is the prior sample covariance of state vector component m and observation y. More details on the DART algorithms and graphical depictions of the algorithm can be found in Anderson et al. (2009).

One common challenge for all ensemble filters, including the EAKF, is insufficient prior variance due to small ensembles, model error, and many other algorithmic deficiencies. This is addressed here using multiplicative inflation of the prior ensemble (Anderson and Anderson, 1999) where the model forecast ensemble is adjusted before the computation of forward operators by

$$x_{m,n}^{inf} = \sqrt{\lambda}(x_{m,n} - \bar{x}_m) + \bar{x}_m, \tag{5}$$

where λ is called a covariance inflation factor.

A second challenge for ensemble filters with small ensemble sizes is spurious sample correlations between weakly correlated observations and state variables. This is addressed using covariance localization (Houtekamer and Mitchell, 2005). The impact of observations on state variables is reduced by introducing a localization factor α in Eq. (4),

$$\Delta x_{m,n} = \alpha\left(\frac{\sigma_{xm,y}}{\sigma_p^2}\right)\Delta y_n. \tag{6}$$

Here, α is a function of the spatial distance between the observation y and the state variable. We use a fifth-order, piecewise continuous and compactly supported function that uses a single parameter to control the radius of influence of an observation (Gaspari and Cohn, 1999). An observation will not influence a state variable that is further away than twice this localization radius. Results of sensitivity experiments with respect to both of the inflation and the width of the localization function are discussed in the next section.

Little information is usually available about the distribution of the initial state (represented by an initial ensemble of state vectors). It is often believed that this should not have an important impact on the long-term behavior of a Bayesian-based filter (Doucet et al., 2001). Hoteit et al. (2008) noticed, however, the importance of including information about the main physical quantities that govern the evolution of the state in the initial ensemble. This could speed up convergence toward the true ocean state while improving the filter's behavior in the early assimilation window. Several methods are available to generate an ensemble of model states for initializing the filter. An ensemble could be generated, for instance, by randomly perturbing a prior estimate of the initial state. This may, however, lead to ensemble members that do not differ in a physically meaningful way. Another way may be to sample an ensemble of state vectors from an established model trajectory. In realistic oceanic data assimilation, the size of the ensemble is often limited by the available computational resources. To ensure that the initial ensemble is representative of the full model phase space, we use the following approach. We first generate a large set of model states that is representative of the full state space by integrating the model over a long period of time. Because we cannot use the whole set of states to initialize the filter, we first apply an Empirical Orthogonal Functions (EOF) analysis to extract the dominant variability from the long model trajectory. The initial ensemble is then generated in the directions of the EOFs using an exact second-order sampling scheme (Pham, 2001; Hoteit et al., 2002). More specifically, if we denote by L_0 the matrix whose r columns are the EOFs, the initial ensemble X_0^i of size $r+1$ is generated with the formula

$$X_0^i = \bar{X} + \sqrt{r+1}L_0\Omega_i^T \tag{7}$$

where $\bar{X}$ is a prior estimate of the state at the initial time (often taken as the mean of the long model trajectory), and Ω_i is the ith of a $(r+1)\times r$ random matrix Ω with orthonormal columns and zero column sums. This drawing amounts to generating an initial ensemble with mean $\overline{X}$ and sample covariance matrix $\tilde{P}_0 = L_0 L_0^T$ that is the best low-rank r approximation of the sample covariance matrix of the original large set of states. The size of the initial ensemble $(r+1)$ is set according to the variance contained in the EOFs and the available computational resources that allow for a reasonable integration time of the ensemble. The ensemble is then used to initialize DART.

3.3. Assimilation experiments and results

Assimilation experiments were performed for a 6-month period in 1999 between May and October during which a strong loop current event occurred (Eddy "Juggernaut") (Oey et al., 2005a). Along-track AVISO SSH anomalies and 25 km gridded TMI SST were assimilated every week with an observation error rms of 5 cm and 0.5 °C, respectively. In the experiments presented below, data were only assimilated within the GoM domain (262–280° E, 18–30° N).

AVISO merges observations from multiple satellites, including ERS-1 and ERS-2, Topex/Poseidon, Jason-1, Jason-2, GFO, and EnviSat, but only the first three satellites were operating during our assimilation period in 1999. The RIO mean dynamic topography, which is a combined product based on GRACE data, altimetry and in-situ data (hydrologic and drifters data) over 7 years (1993–1999) (Rio and Hernandez, 2004), was added to the AVISO anomalies to produce an absolute height. Because we are using a Kalman filtering scheme in this study, which assimilates the data sequentially, the SSH data were binned within the assimilation window before assimilation as if they were available at the middle of this time window. One can also use a smoother approach, which is enabled in DART, to assimilate the data at the time they were taken as in a variational approach. The number of assimilated SSH data at every weekly assimilation cycle varied between 1500 and 2500, with satellites tracks often covering most of the GoM domain. Weekly TMI composites were assimilated in this study. TMI data within 100 km distance from the coast were considered not very reliable and therefore were not assimilated. The absolute SSH signal and the TMI SST were then used to compute the forecast error (or innovation) which was then projected by the filter onto the full space to correct the forecast state.

The EAKF was implemented with different numbers of ensemble members, inflation factors, and localization length scales. We also tested the system under different data configuration and model setups. The results of these experiments are presented and discussed below.

3.3.1. Sensitivity experiments

The sensitivity of the GoM assimilation system to the filter parameters was studied by running the system with various inflation factors and ensemble sizes. We used the same localization scale of 250 km in all the assimilation runs. This radius was chosen after conducting a series of assimilation runs (not shown here) with different localization scales. A large localization radius provided a smoother solution and poorer fit to the data, while a smaller radius provided a better fit to the data but degraded the forecast. The localization scale of 250 km provided the best overall results for the present application and was therefore used in all the experiments presented below.

The sensitivity of the assimilation system to the inflation factor was examined by testing three values: 1.1, 1.2, and 1.3. An ensemble size of 50 was chosen to expedite computation. Because the LCE evolution is mostly traceable by SSH anomalies in the GoM, the performance of the assimilation is mainly assessed by the RMS error between SSH observations and model forecasts/analysis fields and is shown in Fig. 4. The results suggest that inflation plays an important role in the overall performance of the assimilation system. Increasing inflation from 1.1 to 1.2 improves the accuracy of the estimates, especially toward the end of the assimilation window as inflation reduces the spread of the ensemble to allow for uncertainties that were not accounted for in the filter covariances (Hoteit et al., 2002). However, increasing the inflation factor to 1.3 caused some of the ensemble members to diverge during their forward integration with the model. We hypothesize that the increase in the forecast error for the case with the largest inflation is due to a runaway increase in the size of some ensemble members due to a dominance of inflation over the decrease in spread achieved from the observations at each analysis step. The unphysically large variances lead to unphysically large signal-to-noise ratios in the

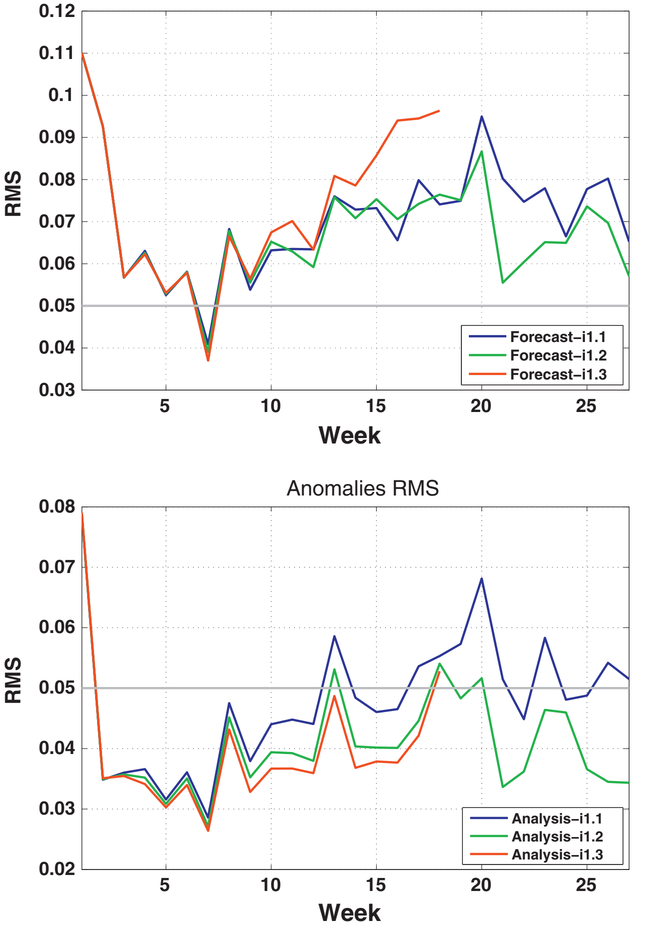

Fig. 4. Exploration of impact of inflation factor with an ensemble size of 50. Root mean square (RMS) misfits between along-track AVISO SSH anomalies and the assimilation solution. Top panel is the 1 week forecast/prior, the bottom panel is the corresponding analysis/posterior (both panels in m). In the legends, "i1.1", "i1.2", and "i1.3" refer to the inflation factors of 1.1, 1.2, and 1.3. The gray line indicates the observational error.

fits, so that observational and representational error are fit as signal, creating spurious adjustments to the ensemble and thus increasingly poor forecasts.

The choice of the ensemble size can be critical to the success of an ensemble-based assimilation system. It must be large enough to accurately represent the mean and spread of the prior distribution, and to allow for the accurate representation of the covariances between the observation and the prior state. However, when the filter is implemented with computationally demanding models, a large ensemble size results in a considerable computational cost. A limited number of ensemble members is therefore inevitable in such systems.

To study the sensitivity of the EAKF assimilation system to the ensemble size and to find the size that provides an acceptable solution at reasonable computational cost, we ran the EAKF with 50, 100, and 200 members. The root-mean-square (RMS) error between SSH observations and model forecasts/analysis fields are shown in Fig. 5. In these runs, the inflation factor is 1.2 and localization radius is 250 km. Increasing the ensemble size decreases the RMS error between model forecasts/analysis and SSH observations, with the assimilation using 200 ensemble members usually having the lowest RMS error for both analysis and forecast. Improvement using 100 members compared to 50 members

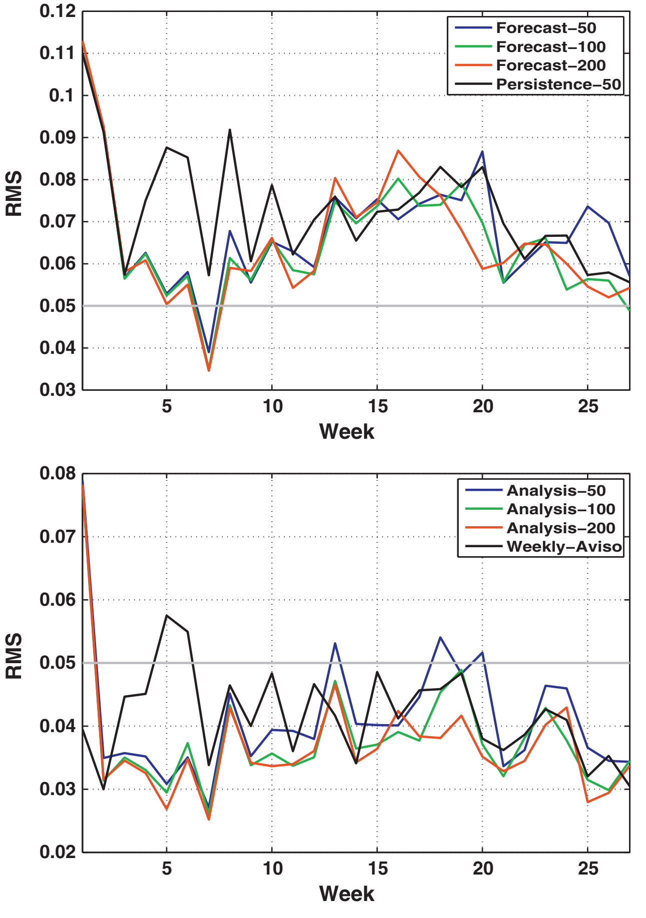

Fig. 5. Exploration of impact of ensemble size with an inflation factor of 1.2. Root mean square (RMS) misfits between along-track AVISO SSH anomalies and the assimilation solution. Top panel is the 1 week forecast/prior, the bottom panel is the corresponding analysis/posterior (both panels in m). Forecast skill is compared to persistence from the filter analysis with 50 ensemble members and analysis skill is compared to RMS misfits from weekly AVISO SSH product. In the legends, "50", "100", and "200" refers to the ensemble size. The gray line indicates the observational error.

is clear, although the solution obtained with 50 members is quite reasonable. There is little to gain when increasing the ensemble size from 100 to 200 to justify doubling the ensemble size (which would almost double the computational cost). The model forecast performance exceeds model persistence most of the time based on the assimilation run with 50 ensemble members. Despite the uncertainties in the RIO mean SSH estimate, the filter analysis resulting from runs with different ensemble sizes also shows improvement when compared with the weekly AVISO merged gridded data. Results not shown here suggest that changes in the ensemble size and the value of the inflation factor had little impact on the filter SST estimates.

We also studied the impact of the assimilated data on the system performance. To this end, we conducted assimilation experiments in which SST and SSH data were assimilated individually and jointly. The results of these experiments are shown in Fig. 6 for the forecast and analysis RMS errors. These assimilation runs used an ensemble size of 50, an inflation factor of 1.2, and a localization radius of 250 km.

When compared to the SSH observations (the left column of Fig. 6), the assimilation of both SSH and SST observations show a RMS misfit very similar to the RMS misfit of assimilating SSH

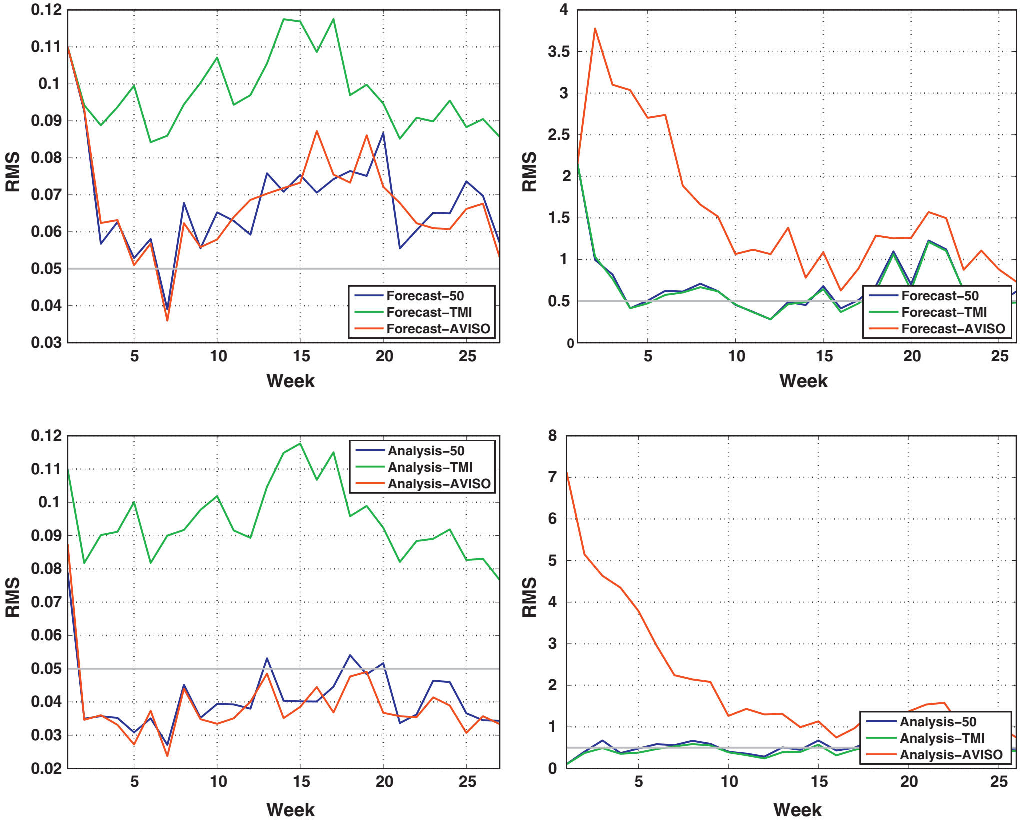

Fig. 6. Root mean square (RMS) misfits among experiments withholding observations. In the legends, "50", "TMI", and "AVISO" refer to runs assimilating both AVISO SSH and TMI SST observations, only TMI SST observations, and only AVISO SSH observations, respectively. *Left panels*: Root mean square (RMS) misfits between along-track AVISO SSH anomalies and the assimilation solutions (top – 1 week forecast, bottom – analysis) in m. *Right panels*: Root mean square (RMS) misfits between TMI SST and the assimilation solutions (top – 1 week forecast, bottom – analysis) in °C. The gray line indicates the observational error.

observations alone. The RMS misfit of the SST-only assimilation is relatively unchanging. This suggests that the assimilation of SST observations has little impact on the estimation of the SSH in the GoM. Slightly better SSH estimates were obtained from only assimilating SSH observations compared to the joint assimilation of SSH and SST observations, but an appropriate tuning/balancing of the prescribed observational error variances for SST and SSH is expected to improve the results of the joint assimilation. The information contained in each data set is different and may explain why the systems response to assimilation of only SST or only SSH is very different. SSH observations are transformed by the assimilation procedure to analysis increments of temperature because changes in SSH are negatively correlated with displacement of isotherms below. The baroclinic adjustment process results in increased SSH matched with downward displacement of isopycnals, and therefore also of the isotherms. This means warmer ocean at the base of the mixed layer, which should increase SST, but only weakly, and only if mixing is active. Other information from SSH could come from changes of the geostrophic currents which alter the advection of heat. The correlation is symmetric, so Just as SSH provides little information about SST because the surface layer is often strongly and stably stratified, SST provides only limited information on the dynamics. A large fraction of the SST error is due to errors in heat flux or mixed layer dynamics and has little effect on SSH; this type of error tends to be at large horizontal scales. In contrast, the SSH error is mainly at the LC scale, resulting from differing eddy growth and shedding. The different scales and signal-to-noise-ratio of the two observation types are the reasons why SSH is able to reduce the SST error at the scales of the LC but not vice versa. The statistics used to create the ensemble show that the subsurface structures that influence SSH, including U and V, and in particular T and S variations, is less correlated with SST than with SSH, which is well-known.

When compared to the SSH observations (the left column of Fig. 6), the assimilation of both SSH and SST observations show a RMS misfit very similar to the RMS misfit of assimilating SSH observations alone. The RMS misfit of the SST-only assimilation is relatively unchanging. This suggests that the assimilation of SST observations has little impact on the estimation of the SSH in the GoM. Slightly better SSH estimates were obtained from only assimilating SSH observations compared to the joint assimilation of SSH and SST observations, but an appropriate tuning/balancing of the prescribed observational error variances for SST and SSH is expected to improve the results of the joint assimilation. The information contained in each data set is different and may explain why the systems response to assimilation of only SST or only SSH is very different. SSH data provides information resulting from the assimilation procedure as analysis increments of temperature because changes in SSH are negatively correlated with displacement of isotherms below, and information resulting from changed circulation on the SST. The baroclinic adjustment process leads to the relation of increased SSH together with a downward displacement of the isopycnals, and therefore also of the isotherms. This means warmer ocean at the base of the mixed layer, which directly impact SST. Other information from SSH could come from changes of the geostrophic currents which alter the advection of heat. On the other hand, SST provides only limited information on the dynamics and may only alter the SSH on the large scale. Indeed, a large fraction of the SST error is due to errors in heatflux or mixed layer dynamics and has little effect on SSH; this type of error is more large scale. In contrast, the largest fraction of the SSH error is mainly at scale of the LC resulting from different eddy growth and shedding. This error imprints also on SST. This could explain why SSH is able to improve the fraction of the SST error on scales of LC but not vice versa. The statistics used to create the ensemble show that the subsurface structure is less correlated with SST than with SSH, which is well-known.

The inference is quite different if measured against the SST observations (the right column of Fig. 6). The assimilation of only SSH observations has a considerable impact on both the analysis and the forecast quality of SST. It is interesting to note that the performance gradually improves over the first 10 weeks, reaching a level which is about twice the RMS obtained with the combined SSH and SST assimilation. There are at least two reasons for the gradual improvement. The advection of heat that follows the loop current and the upper ocean advection velocities are well constrained by the SSH observations. This mechanism also provides an explanation for the time scale of a few months which is typical for eddy advection. The multivariate nature of the ensemble Kalman filter allows for direct improvement of the SST through assimilation of SSH during the analysis step. However, the experiment of assimilating only SST demonstrates that this is probably not very efficient.

The sensitivity of the assimilation system to uncertainties in the forcing fields and the open boundary conditions (OBCS) are examined by perturbing the forcing and OBCS separately. In these runs, the system used forcing and OBCS from 1998 (the year before), an ensemble size of 50, an inflation factor of 1.2, a localization radius of 250 km, and assimilated both SST and SSH observations. The RMS error evolution for model forecasts and analyses are shown in Fig. 7. Compared to the SSH observations, it shows that before week 20 the 1998 forcing and OBCS cases perform within about 1 cm RMS difference of the true forcing and OBCS, and are about equally likely to be better as worse. On week 20, the OBCS case is 2 cm RMS worse, and on week 21, both OBCS and forcing are about 2 cm worse. After that the difference declines and forcing and OBCS cases even outperform slightly during the last 3 weeks. In the analysis, the incorrect OBCs and forcing systematically increase the RMS difference, by a maximum of about 2.5 cm RMS on day 20 for the OBCS case. When compared to the SST observations, perturbing the forcing has a noticeable impact on the RMS differences while perturbing the OBCS has little effect. However, further examination of the estimated circulation suggests that these seem to remain transient, affecting only the near surface without significantly disturbing the circulation. In summary, the RMS error for these perturbed assimilation runs indicates that there is some sensitivity to the forcing and OBCS fields, but it is generally not large for the forecasts, and more realizations would be needed to give good statistics for a generalization. Reported experiments indicate that the system is sufficiently constrained by observations of SSH and SST and appropriate initial conditions to be useful for the predictability of the GoM circulation on the time scales considered here. A future enhancement

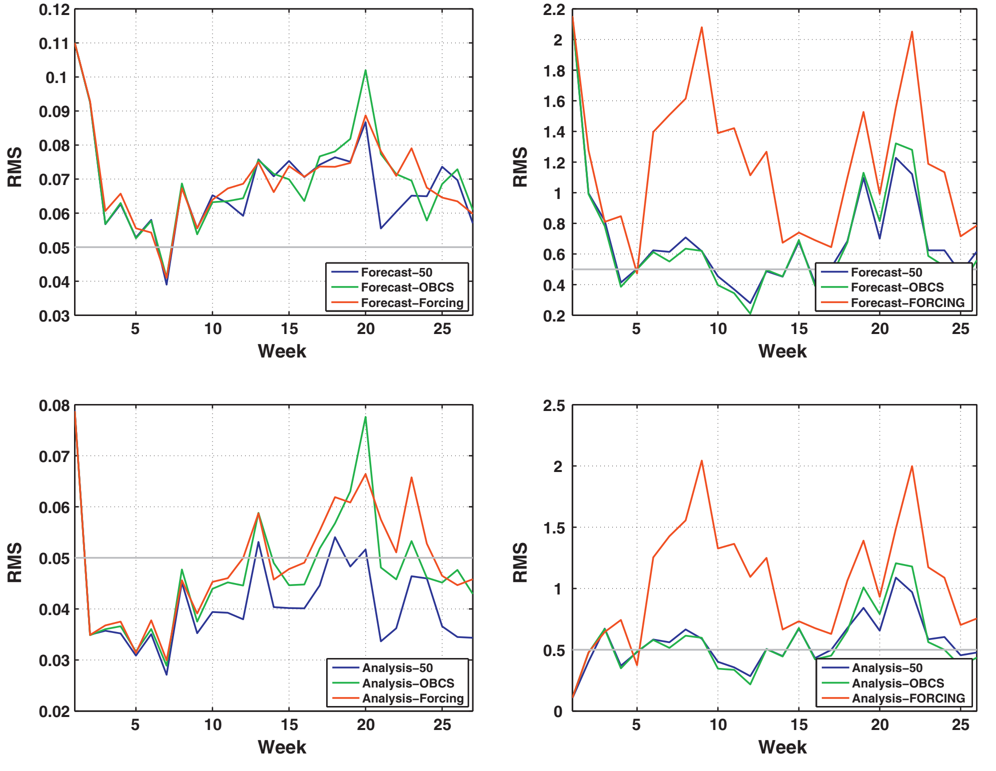

Fig. 7. Root mean square (RMS) misfits among perturbation experiments. In the legends, "50", "OBCS", and "Forcing" refer to runs with the correct initial conditions, perturbed open boundary conditions and forcing fields from 1998 (the previous year), respectively. *Left panels*: Along-track AVISO SSH misfit in m (top – 1 week forecast, bottom – analysis). *Right panels*: TMI SST misfit in °C (top – 1 week forecast, bottom – analysis). The gray line indicates the observational error.

to the assimilation system would be to include uncertainty in the forcing fields, and secondarily OBCS, by having different values for each of the ensemble members. This would somehow account for model deficiencies and help maintaining the ensemble spread in the GoM model as suggested by Counillon and Bertino (2009b).

3.3.2. *Estimated state*

The ensemble mean SSH forecasts and analyses from the assimilation experiment using 100 ensemble members, an inflation factor of 1.2, and a localization radius of 250 km were compared to AVISO SSH products and are shown in Fig. 8. The range of times was selected to highlight the separation of eddy "Juggernaut". Also shown in the right column is the ensemble mean analysis from an assimilation using 50 ensemble members. The 1 week forecasts from the DART/MITgcm assimilation (the second column) accurately predict the SSH from the AVISO product. The northward extension of the LC into the GoM, the eddy separation, and "re-attachment" (not visible from the figure) events are well reproduced. The solution of the 50 ensemble members run is quite reasonable, correctly reproducing the evolution of the LC. However, using more members provides more details of the GoM circulation. For instance, the fine structure of cyclonic rings adjacent to the anti-cyclonic LCE before and after the ring separation is more sharply defined in the 100 ensemble run than in the 50 ensemble run. One can also notice the large improvement to the initial state estimate obtained by the first data assimilation step. Compared to a model free-run without assimilation, the filter improved the model SSH by about 9 cm and the model SST by more than 0.5 °C on average.

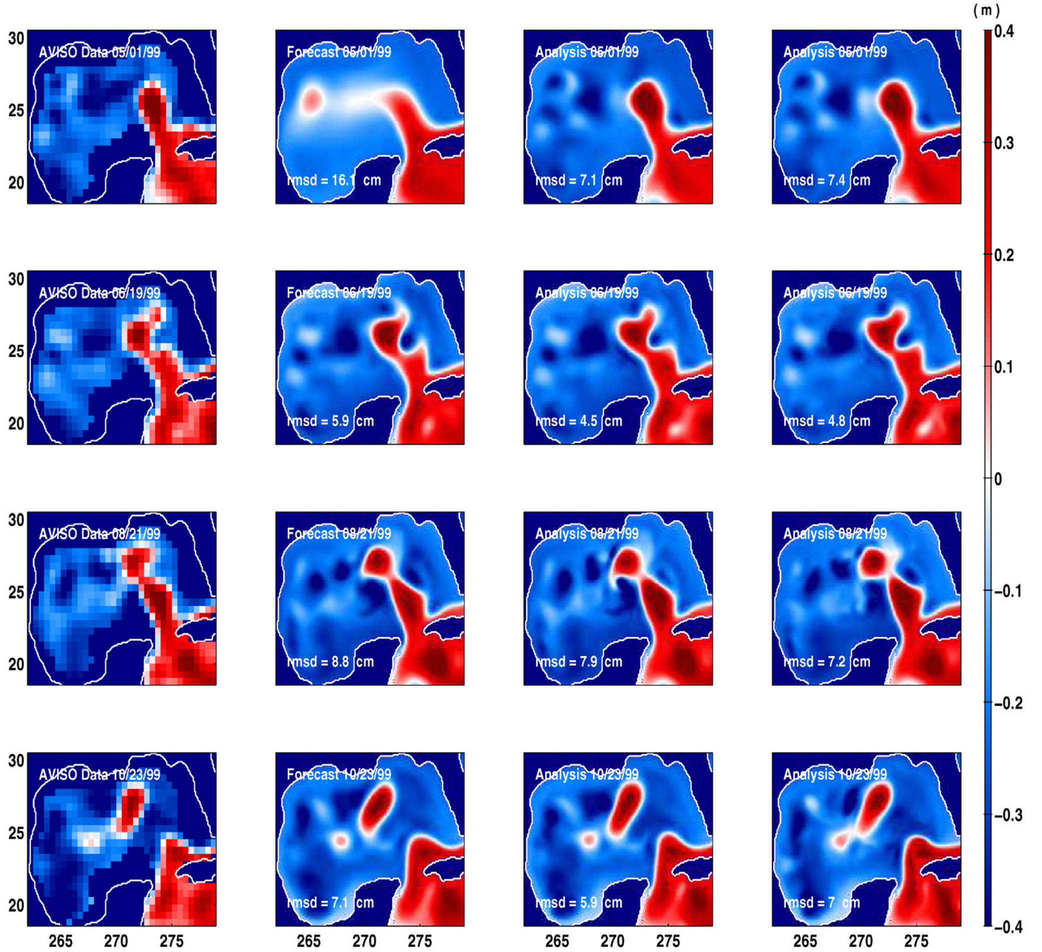

Fig. 8. Comparison of ensemble mean SSH to the weekly AVISO SSH gridded product. The rows represent dates selected to highlight an eddy separation event. The first/left column is the AVISO SSH product. The second column is the ensemble mean of the 1 week forecast from the assimilation with 100 ensemble members. The third column is the analysis/posterior ensemble mean for that date. The fourth column is the ensemble mean of the analysis from a run with 50 ensemble members. The horizontal RMS estimation error is provided in the low left corner of each panel. Units are m.

The ensemble mean SST forecasts and analyses were also compared to the 25 km gridded weekly TMI SST product and are shown in Fig. 9. In contrast with the SSH, estimates of SST are not substantially different between the 50- and 100-member ensemble runs. The TMI product resolution precludes many details of the loop current and appears somewhat noisy in comparison to the assimilation solution. On June 19, the LCE features are not well resolved in the TMI product, while model forecasts and analyses clearly defined northward-extending features. DART/MITgcm forecasts and analyses for August 21 also clearly show a more pronounced estimate of the LCE signature than the TMI product. This suggests that the DART/MITgcm assimilation provides additional details consistent with the observations and data in the GoM compared to the gridded TMI product.

Fig. 10 plots the ensemble spread (or ensemble RMS) for the SSH and SST as it results from the assimilation run with 100 ensemble members at the same selected dates as for the means. Starting with climatological ensemble spread with mainly large-scale spatial variability at the initial time, the filter analysis quickly reduces the ensemble spread after the first assimilation cycle for both SSH

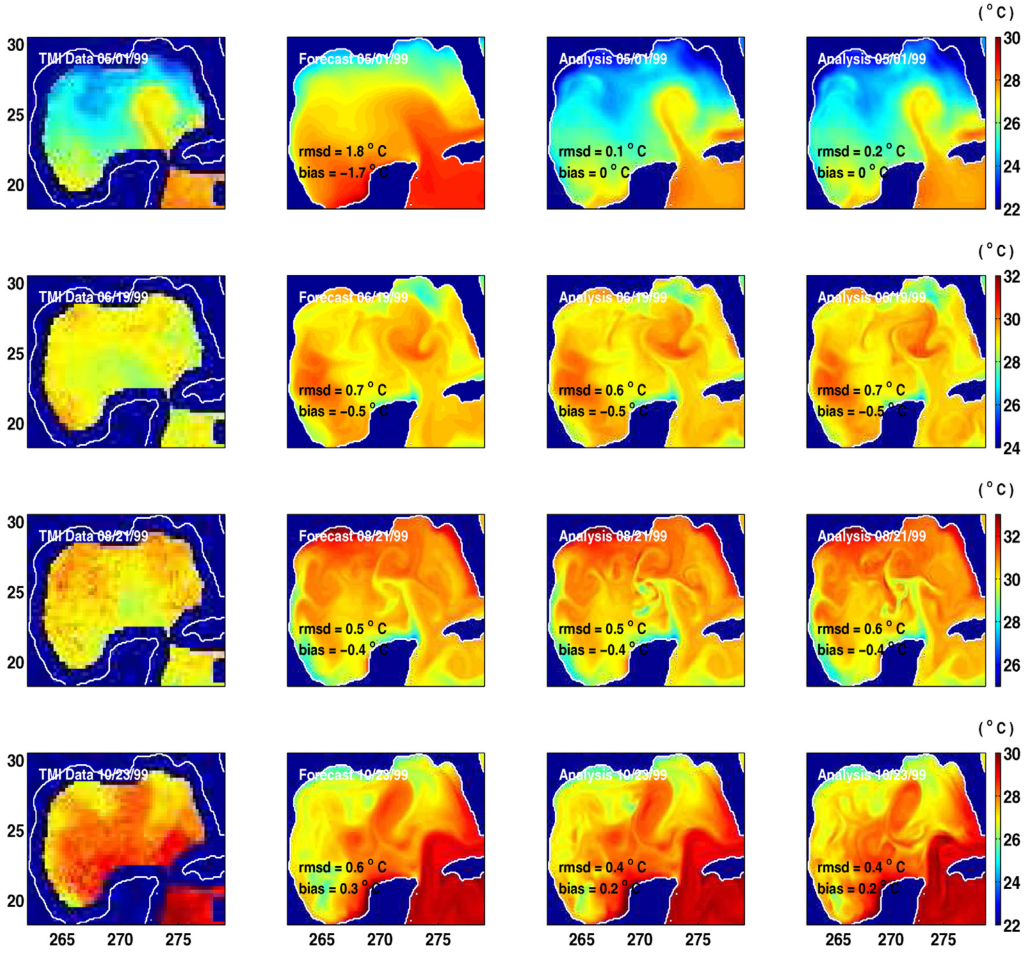

Fig. 9. Same as Fig. 7 for ensemble mean SST compared to weekly TMI SST gridded product. The horizontal RMS estimation error and associated horizontally averaged time-mean bias are provided in the low left corner of each panel. Units are °C.

and SST. The effects of the along-track SSH observations are clear in the first analysis spread, which shows the tracks and spread that remains high in a region without samples. For SSH, the ensemble spread after the forecast step is generally concentrated around the fronts of the loop current and the associated shedded eddies, indicating largest forecast uncertainties in these areas. This is also visible from the spread of the SST ensemble, which also exhibits large spread in the south–west, possibly due to westward propagating features. The filter analysis step reduces the spread after every assimilation cycle, and the remaining spread is dominated by filaments of variability. The temporal evolution of the spread seems to be steady; increasing and then decreasing by similar amounts after each forecast and analysis step, respectively.

The impact of data assimilation on the three-dimensional currents is also studied by evaluating the mean along-channel velocity field across the Yucatan Channel as it results from different runs against the basic known features of the flow in this area. Here we focus on the XZ vertical section at 21.85° N. The predominant features of the mean-currents across the Yucatan Channel consists of the northerly Yucatan Current in the upper western layers of the channel flowing from the Caribbean Sea into GoM and its deep southerly under-current off Mexico, and southerly Cuban counter-current near the surface and at deeper layers on the eastern side of the channel (near Cuba) (Sheinbaum et al., 2002; Ochoa

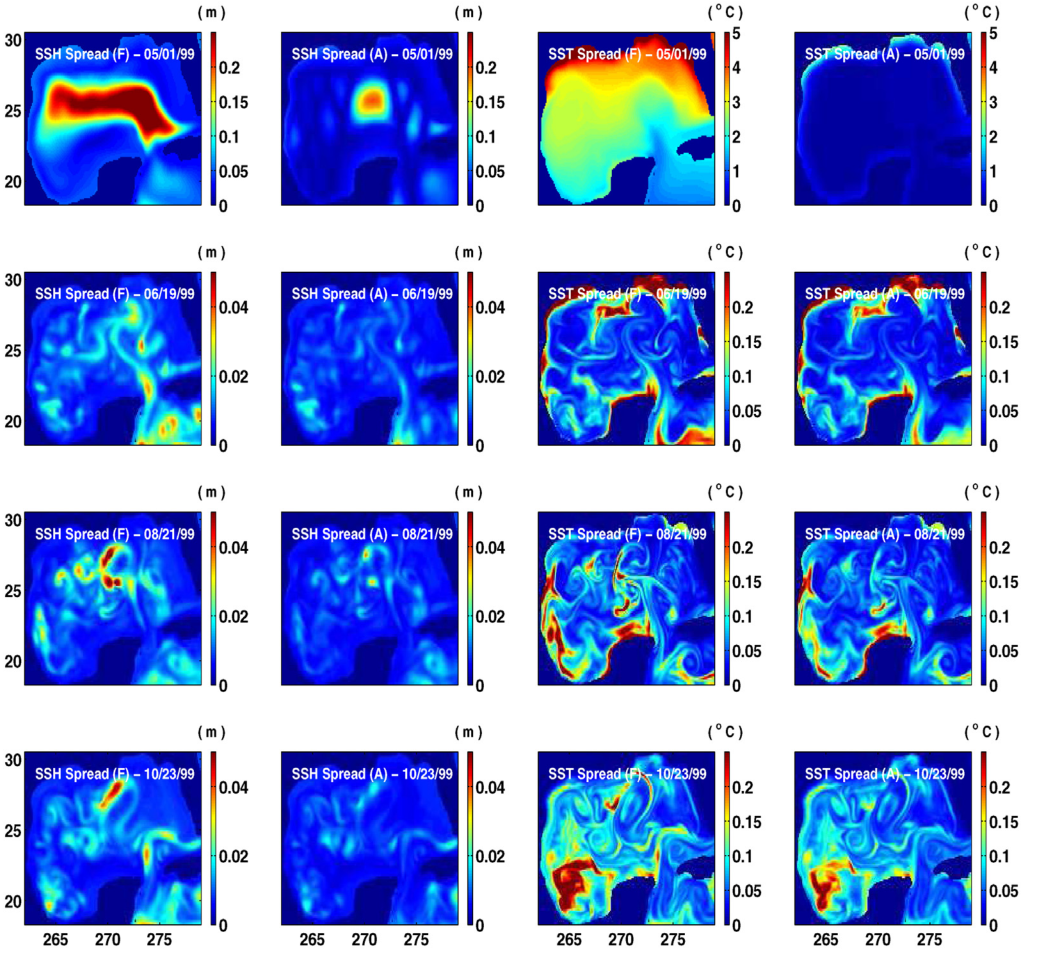

Fig. 10. Spread of the SSH forecast (1st column) and analysis (2nd column), and of SST forecast (3rd column) and analysis (4th column). Units are in m for SSH and in °C for SST. The rows represent dates selected to highlight an eddy separation event.

et al., 2001; Candela et al., 2002). Mean meridional velocity fields across the Yucatan Channel were computed over the assimilation period (May-October, 1999) and are shown in Fig. 11(a)–(d), for the following assimilation runs: (1) model free-run without assimilation, (2) filter analysis assimilating SST and SSH data using 50 ensemble members, (3) filter analysis assimilating only SST data, and (4) filter analysis assimilating only SSH data. The model simulation without assimilation (Fig. 11(a)) shows the northward inflow into the GoM in the upper western layers of the channel and the southerly surface Cuban counter-current on the eastern side, but fails to represent the deep southward Yucatan Counter-current along the western slope of the channel. The filter solution with assimilation of SST and SSH data (Fig. 11(b)) and 50 ensemble members shows the northward Yucatan current in the upper western layers of the channel and the southward counter-current at deeper layers beneath it, as well as the southward Cuban counter-current near the surface and at deeper layers along with a northward inflow at mid-depths on the eastern side of the channel seen in at certain times in observations (e.g. Abascal et al., 2003). However, a detailed verification is not possible due to lack of observations for this period. Assimilation of only TMI-SST data provides similar structures, but fails to represent the southward surface Cuban counter-current (Fig. 11(c)). Assimilation of only SSH data seems to provide a more consistent flow through the Yucatan Channel (Fig. 11(d)) with that analyzed from the

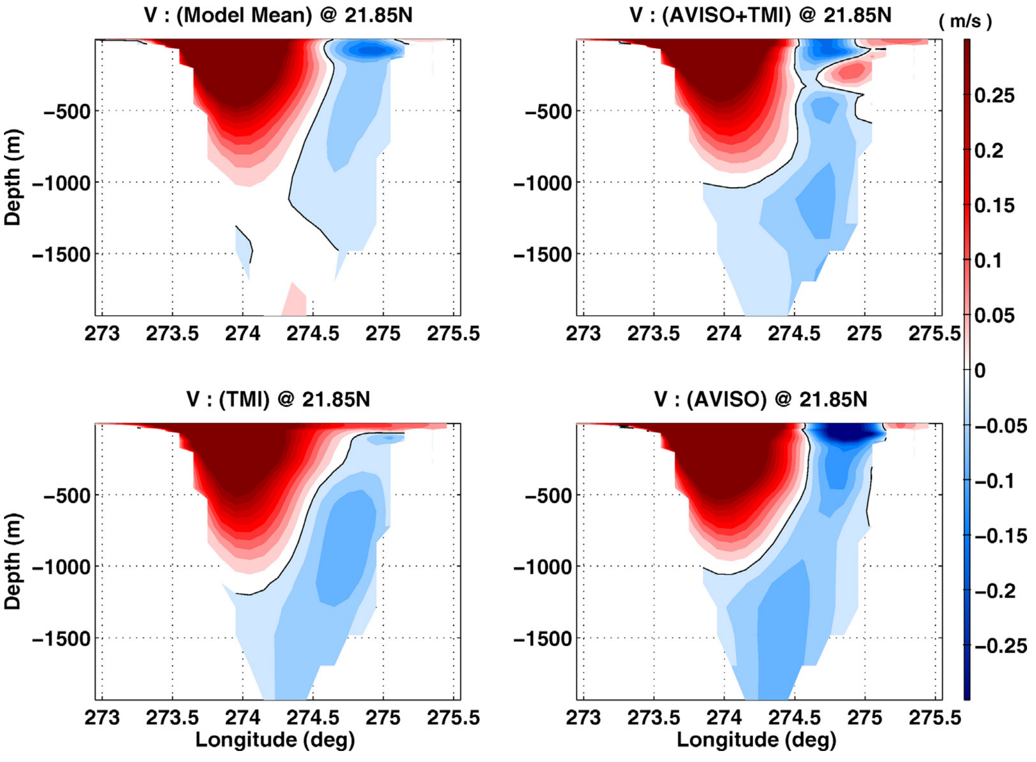

Fig. 11. Cross *XZ* vertical section of the mean velocity field along the Yucatan channel at 21.85° N from (a) model run without assimilation, and filter runs with assimilation of (b) AVISO SSH and TMI SST data, (c) only TMI SST data, and (d) only AVISO SSH data. Black line represents the 0 m/s contour.

CANEK observations (e.g. Ochoa et al., 2001; Sheinbaum et al., 2002). Compared with the solution assimilating both SSH and SST, it results in an increased northward surface inflow on the western (Mexican) side of the channel but fails to produce the northward inflow at mid depths along the eastern side of the channel. Overall, the impact of assimilation of surface-only data is positive in all cases, but most pronounced when SSH data are assimilated, with the filter successfully propagating the surface information to the deep ocean.

3.3.3. Dynamical balance of estimates

A discussion of the impact of the ensemble data assimilation on the dynamical balance of the state estimates is warranted. The ensemble forecasts are model outputs and are therefore equilibrated with the model dynamics by construction. The ensemble mean of the forecast state is not. The analysis state is the sum of the forecast state and the Kalman projection of the forecast residuals into the state space using the gain matrix. The larger this correction to the forecast, and the more localization is used to alter the ensemble covariance, the less dynamically balanced the analysis state is expected to be. It is generally hoped that, for well-observed ensemble-based assimilation systems, corrections become smaller over time as the filter estimates become closer to the observations (Kepert, 2009).

We examined the dynamical balance of the forecast and analysis (before any time-stepping with the model) during the assimilation, showing an example near the end of the assimilation. The goal of this section is twofold: (i) give more insight about the dynamical balances of the LC, and (ii) provide another way to assess the performance of the assimilation system. One concern with state estimates from a Kalman-based filter is that even though observed features may be accurately reproduced, the dynamical balances may be distorted. It is not our intention to study the dynamical balance of the GoM in full detail, but to demonstrate that the successive correction steps of the EnKF are not obviously distorting the dynamics of the model. Examining the momentum terms for the total analysis instead of the correction alone puts the terms in context of the flow, although it dilutes the focus on imbalances in the corrections. The total model state is what is integrated forward, and so is what matters practically. Obviously, a tiny correction can be far out of balance without affecting the total balances. The total fields serve both to diagnose the size of the imbalance due to the assimilation and to see the typical terms in the loop current dynamics.

The terms in the momentum equation are calculated from the analysis velocity and pressure fields, leaving out the Reynolds stress divergences and the current acceleration terms. Analysis fields are chosen because they are more likely to show perturbations to the true balance than the forecast, which has time to adjust dynamically. Both forecast (not shown) and analysis balances were evaluated, and only small (less than 5%) differences between forecast and analysis were seen, supporting the presumption that the corrections imposed by the assimilation are 'small'. This can also be seen by comparing forecast and analysis snapshots from Figs. 8 and 9.

The MITgcm uses the flux form to calculate the momentum advection terms, but the individual terms have been estimated separately offline. The example shown in Fig. 12 is for the 24th analysis, and is the starting state for the 25th forecast before time-stepping, so the mismatch between the Coriolis force and the other terms (lumped together as "right-hand side" or RHS) in the figures is the tendency term in the first time-step. The tendency term can be large if the adjustments made by the filter are not geostrophically balanced, leading to fast-propagating inertial and internal gravity waves which can hurt the model skill. The flow is expected to be near geostrophic or cyclostrophic balance, and this is generally true for both averages and snapshots of forecast or analysis fields. The momentum equations can be written as a balance between the Coriolis force and all the other terms as

$$-fv = -\frac{\partial u}{\partial t} - \mathbf{u} \cdot \nabla u - \frac{\partial \phi}{\partial x} + a_x$$
$$fu = -\frac{\partial v}{\partial t} - \mathbf{u} \cdot \nabla v - \frac{\partial \phi}{\partial y} + a_y$$

where ϕ is the dynamic pressure, $\mathbf{u}$ is the 3-D velocity, f is the Coriolis parameter, and a_x and a_y are the residual forces. Selected terms in the momentum equation for the 24th analysis step are sampled along a section at 26° N for two depths, 37 m and 204 m, chosen to be below the surface mixing and to span the depth extent of the strong currents (Fig. 12). This section is chosen to cross the loop current in a region where an eddy is forming. The strong northward current centered at about 270.5° E and the nearly equal return southward current at about 272.5° E are visible in the $-Fv$ curve plotted in the top panel. The parameterized vertical and horizontal friction terms were negligible in these balances.

Both zonal and meridional budgets show nearly geostrophic balance, as expected, with the advection terms only important in the regions of high currents and gradients. The flow is weaker at 204 m, but has similar shapes and balances. The vertical advection of the vertical gradient of horizontal momentum is zero in the initialization, which can add to the imbalance. However, this term is small in the model simulations, where the vertical shears times the vertical velocities (not shown) are small (less than 3% of a typical Coriolis term), so it is not expected to be important. This may be due to the relatively coarse grid used in this study. There is a residual difference between the Coriolis term (green line) and the summed mean accelerations (red line) due to the neglected terms, but the balances are not obviously distorted. In addition to the check of balance, the momentum terms show the importance of the nonlinear terms in the regions with strong currents and horizontal shear.

4. Discussion

We have described the development of an advanced ensemble Kalman filter (EnKF)-based ocean assimilation system to predict the evolution of the loop current in the Gulf of Mexico (GoM). The system is composed of the MIT general circulation model (MITgcm) and the Data Assimilation Research Testbed (DART) and is suitable for high-resolution basin-wide and coastal oceanic applications. The system supports different EnKFs and smoothers, can be used for parameter estimation, and is

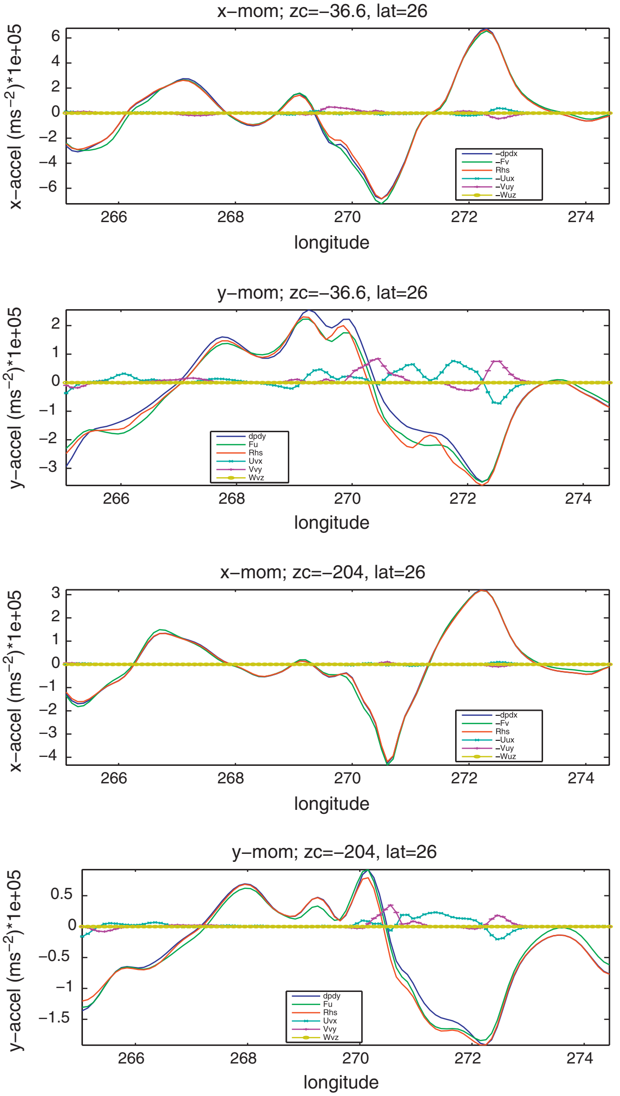

Fig. 12. Dynamical balance of filter estimate after 24 analysis steps (toward the end of the assimilation). Panels are (top to bottom): *x*- and *y*-momentum for 37 m depth, *x*- and *y*-momentum for 204 m depth. In all panels, the blue curve is pressure gradient, the green curve is Coriolis force, the red curve is the pressure gradient term plus advection terms. The advection terms are also plotted separately: the cyan curve with the "x" symbols is the zonal advection of zonal momentum, the magenta curve with the "square" symbols is the meridional advection of zonal momentum, and the gold curve with the "o" symbols is the vertical advection of zonal momentum. Derivatives terms of *W*(*Wuz*, *Wvz*) are neglected and marked as zero in the plots (color yellowish brown). (For interpretation of the references to color in this figure legend, the reader is referred to the web version of the article.)

further enabled for assimilation of most ocean observations. To the best of our knowledge, this is the first advanced ensemble Kalman-based ocean assimilation system that is freely available and well documented.

In the GoM prediction system, the ensemble adjustment Kalman filter (EAKF) was used to assimilate weekly along-track satellites sea surface height (SSH) and sea surface temperature (SST) observations into an eddy-permitting 1/10 degree configuration of the MITgcm in the GoM. We found that the system with 100 ensemble members exhibits relatively high forecast skill, and is more accurate (by about 13%) than persistence of the flow. Increasing the ensemble size from 100 to 200 was not crucial for the loop current prediction. The estimated state of the GoM was also found to be smoother than mapped SST and SSH products from TMI and AVISO, reproducing the signature of the LC with greater detail. These results suggest that this ensemble-based system is able to extract the dynamically important information from the model to provide reliable statistics to map the information from the observations into the model space and generate a good initialization for the ensemble forecast. The assimilation system although exhibited some sensitivity to forcing and open boundaries, but it is generally not large for the forecasts, and more realizations would be needed to give good statistics for a generalization. On the timescales considered, the quality of the predicted state mainly depends on the initial conditions. The analysis of the dynamical balance of the forecast and analysis states also demonstrates that the dynamical balance of the LC is in general agreement with previous studies and that the EAKF's analysis only weakly affects the dynamical balance of the system.

The newly developed MITgcm/DART system will complement the ECCO adjoint-based system, providing a dynamically evolving background covariance matrix and schemes less sensitive to the strong nonlinearities of high resolution configurations. This should further open new perspectives for developing and implementing hybrid ocean variational-ensemble assimilation systems; an approach that is becoming popular because of its inheritance of the desirable properties of the two assimilation approaches (Liu et al., 2008; Zhang et al., 2009). Future work will mainly focus on improving the forecast skill of the GoM assimilation system, testing the different features of the DART/MITgcm assimilation system, and developing and implementing new assimilation schemes using the existing adjoint- and ensemble-based assimilation systems.

References

Abascal, A., Sheinbaum, J., Candela, J., Ochoa, J., Badan, A., 2003]. Analysis of flow variability in the Yucatan Channel. J. Geophys. Res 108 (10.1029).

Aksoy, A., Dowell, D.C., Snyder, C., 2009]. A multicase comparative assessment of the ensemble Kalman filter for assimilation of radar observations. part I: storm-scale analyses. Mon. Wea. Rev. 137, 1805–1824.

Anderson, J., 2001]. An ensemble adjustment kalman filter for data assimilation? Mon. Wea. Rev. 129 (12), 2884–2903.

Anderson, J., 2003]. A local least squares framework for ensemble filtering. Mon. Wea. Rev. 131, 634–642.

Anderson, J., Anderson, S., 1999]. A Monte Carlo implementation of the nonlinear filtering problem to produce ensemble assimilations and forecasts. Mon. Wea. Rev. 127 (12), 2741–2758.

Anderson, J., Hoar, T., Raeder, K., Liu, H., Collins, N., Torn, R., Arellano, A., 2009]. The data assimilation research testbed: a community facility? Bull. Amer. Meteorol. Soc. 90 (9), 1283–1296.

Anderson, J.L., Collins, N., 2007]. Scalable implementations of ensemble filter algorithms for data assimilation? J. Atmos. Ocean. Technol. 24 (8), 1452–1463.

Bennett, A.F., 2002]. Inverse Modeling of the Ocean and the Atmosphere. Cambridge Univ. Press, New York.

Candela, J., Sheinbaum, J., Ochoa, J., Badan, A., Leben, R., 2002]. The potential vorticity flux through the Yucatan channel and the loop current in the Gulf of Mexico? Geophys. Res. Lett. 29 (22), 16-1.

Chassignet, E., Hurlburt, H., Smedstad, O., Halliwell, G., Hogan, P., Wallcraft, A., Baraille, R., Bleck, R., 2007]. The Hycom (hybrid coordinate ocean model) data assimilative system. J. Mar. Syst. 65, 60–83.

Counillon, F., Bertino, L., 2009a]. Ensemble optimal interpolation: multivariate properties in the Gulf of Mexico? Tellus - A 61 (2), 296–308.

Counillon, F., Bertino, L., 2009b]. High-resolution ensemble forecasting for the Gulf of Mexico eddies and fronts? Ocean Dyn. 59 (1), 83–95.

Counillon, F., Sakov, P., Bertino, L., 2009]. Application of a hybrid enkf-oi to ocean forecasting? Ocean Sci. 5 (1), 389–401.

Doucet, A., de Freitas, N., Gordon, N., 2001]. Sequential Monte Carlo Methods in Practice. Springer, New York, p. 581.

Dowell, D.C., Wicker, L., 2009]. Additive noise for storm-scale ensemble data assimilation. J. Atmos. Ocean. Technol. 26, 911–927.

Fan, S., Oey, L., Hamilton, P., 2004]. Assimilation of drifter and satellite data in a model of the northeastern Gulf of Mexico? Continental Shelf Res. 24 (9), 1001–1013.

Gaspari, G., Cohn, S., 1999]. Construction of correlation functions in two and three dimensions. Quart. J. Roy. Meteorol. Soc. 125, 723–757.

Ghil, M., Malanotte-Rizzoli, P., 1991]. Data assimilation in meteorology and oceanography. Adv. Geophys. 33, 141–266.

Heimbach, P., Hill, C., Giering, R., 2002]. Automatic generation of efficient adjoint code for a parallel Navier–Stokes solver. In: Dongarra, J.J., Sloot, P.M.A., Tan, C.J.K. (Eds.), In: Lecture Notes in Computer Science (LNCS), vol. 230 (Part II). Springer-Verlag, pp. 1019–1028.

Hoteit, I., Luo, X., Pham, D.-T., 2012]. Particle Kalman filtering: a nonlinear Bayesian framework for ensemble Kalman filters. Mon. Wea. Rev. 140, 528–542.

Hoteit, I., Pham, D., Blum, J., 2002]. A simplified reduced order Kalman filtering and application to altimetric data assimilation in tropical pacific. J. Mar. Syst. 36, 101–127.

Hoteit, I., Pham, D.-T., Triantafyllou, G., Korres, G., 2008]. A new approximate solution of the optimal nonlinear filter for data assimilation in meteorology and oceanography. Mon. Wea. Rev. 136, 317–334.
Houtekamer, P., Mitchell, H., 2005]. Ensemble Kalman filtering. Quart. J. Roy. Meteorol. Soc. 131, 3269–3289.
Kalnay, E., Kanamitsu, M., Kistler, R., Collins, W., Deaven, D., Gandin, L., Iredell, M., Saha, S., White, G., Woollen, J., et al., 1996]. The NCEP/NCAR 40 reanalysis project. Bull. Amer. Meteorol. Soc. 77, 437–471.
Kantha, L., Choi, J., Schaudt, K., Cooper, C., 2005]. A regional data-assimilative model for operational use in the Gulf of Mexico. Geophys. Monogr. – Am. Geophys. Union 161, 165–180.
Kepert, J., 2009]. Covariance localisation and balance in an ensemble Kalman filter. Quart. J. Roy. Meteorol. Soc. 135, 1157–1176.
Köhl, A., Stammer, D., 2008]. Variability of the meridional overturning in the north atlantic from the 50 years gecco state estimation. J. Phys. Oceanogr. 38, 1913–1930.
Large, W., McWilliams, J., Doney, S., 1994]. Oceanic vertical mixing: a review and a model with a nonlocal boundary layer parameterization. Rev. Geophys. 32, 363–403.
Le Dimet, F.X., Talagrand, O., 1986]. Variational algorithms for analysis and assimilation of meteorological observations: theoretical aspects. Tellus 38, 97–110.
Leben, R., 2005]. Altimeter-derived loop current metrics. Geophys. Monogr. – Am. Geophys. Union 161, 181–201.
Levitus, S., Boyer, T., 1994. World Ocean Atlas 1994. NOAA atlas NESDIS, 3–4: US Govt Printing Office, Washington, DC.
Lin, X., Oey, L., Wang, D., 2007]. Altimetry and drifter data assimilations of loop current and eddies. J. Geophys. Res. 112 (C11), 05046.
Liu, C., Xiao, Q., Wang, B., 2008]. An ensemble based four-dimensional variational data assimilation scheme. Part I: technical formulation and preliminary test. Mon. Wea. Rev. 136 (9), 3367–3376.
Marshall, J., Adcroft, A., Hill, C., Perelman, L., Heisey, C., 1997]. A finite-volume, incompressible Navier–Stokes model for studies of the ocean on parallel computers. J. Geophys. Res. 102, 5753–5766.
McDougall, T.J., Jackett, D.R., Wright, D.G., Feistel, R., 2003]. Accurate and computationally efficient algorithms for potential temperature and density of seawater? J. Atmos. Ocean. Technol. 20 (5), 730–741.
Nerger, L., Hiller, W., Schröter, J., 2005]. The parallel data assimilation framework: experiences with Kalman filtering. In: Zwieflhofer, W., Mozdzynski, G. (Eds.), Use of High Performance in Meteorology, Proceedings of the 11th ECMWF Workshop. World Scientific, Singapore, pp. 63–86.
Ngodock, H., Smith, S., Jacobs, G., 2007]. Cycling the representer algorithm for variational data assimilation with a nonlinear reduced gravity ocean model? Ocean Model. 19 (3–4), 101–111.
Nof, D., 2005]. The momentum imbalance paradox revisited? J. Phys. Oceanogr. 35 (10), 1928–1939.
Ochoa, J., Sheinbaum, J., Badan, A., Candela, J., Wilson, D., 2001]. Geostrophy via potential vorticity inversion in the Yucatan Channel. J. Mar. Res. 59, 725–747.
Oey, L., Ezer, T., Forristall, G., Cooper, C., DiMarco, S., Fan, S., 2005a]. An exercise in forecasting loop current and eddy frontal positions in the Gulf of Mexico. Geophys. Res. Lett. 32 (12), L12611.
Oey, L., Ezer, T., Lee, H., 2005b]. Loop current, rings and related circulation in the Gulf of Mexico: a review of numerical models and future challenges. Geophys. Monogr. – Am. Geophys. Union 161, 31.
Ohlmann, J., Niiler, P., Fox, C., Leben, R., 2001]. Eddy energy and shelf interactions in the Gulf of Mexico. J. Geophys. Res. 106, 2605–2620.
Pham, D., 2001]. Stochastic methods for sequential data assimilation in strongly nonlinear systems. Mon. Wea. Rev. 129, 1194–1207.
Powell, B., Arango, H., Moore, A., Di Lorenzo, E., Milliff, R., Foley, D., 2008]. 4dvar data assimilation in the intra-americas sea with the regional ocean modeling system (roms)? Ocean Model. 23 (3–4), 130–145.
Rio, M.-H., Hernandez, F., 2004]. A mean dynamic topography computed over the world ocean from altimetry, in situ measurements, and a geoid model. J. Geophys. Res. 109 (C1), 2032.
Sheinbaum, J., Candela, J., Badan, A., Ochoa, J., 2002]. Flow structure and transport in the Yucatan channel? Geophys. Res. Lett. 29 (3), 10–11.
Srinivasan, A., Chassignet, E., Bertino, L., Brankart, J., Brasseur, P., Chin, T., Counillon, F., Cummings, J., Mariano, A., Smedstad, O., Thackerd, W., 2001]. A comparison of sequential assimilation schemes for ocean prediction with the hybrid coordinate ocean model (hycom): twin experiments with static forecast error covariances. Ocean Model. 37, 85–111.
Stammer, D., Chassignet, E., 2000]. Ocean state estimation and prediction in support of oceanographic research. Oceanography 13, 51–56.
Tippett, M., Anderson, J., Bishop, C., Hamill, T., Whitacker, J., 2003]. Ensemble square root filters. Mon. Wea. Rev. 131, 1485–1490.
Vukovich, F., 1995]. An updated evaluation of the loop current's eddy-shedding frequency. J. Geophys. Res. 100 (C5), 8655–8659.
Wunsch, C., 1996]. The Ocean Circulation Inverse Problem. Cambridge Univ. Press, New York.
Yin, X., Oey, L., 2007]. Bred-ensemble ocean forecast of loop current and rings? Ocean Model. 17 (4), 300–326.
Yu, P., Morey, S., O'Brien, J., 2009]. A reduced-dynamics variational approach for the assimilation of altimeter data into eddy-resolving ocean models? Ocean Model. 27 (3–4), 215–229.
Zhang, F., Zhang, M., Hansen, J.A., 2009]. Coupling ensemble Kalman filter with four-dimensional variational data assimilation? Adv. Atmos. Sci. 26 (1), 1–8.
Zubrow, A., Chen, L., Kotamarthi, V., 2008]. Introduction and evaluation of a data assimilation for cmaq based on the ensemble adjustment Kalman filter. J. Geophys. Res. 113, D09302, http://dx.doi.org/10.1029/2007JD009267.